PROCEEDINGS A

royalsocietypublishing.org/journal/rspa

Research

Cite this article: Padhi E, Ali SZ, Dey S. 2019 Mechanics of bed particle saltation in turbulent wall-shear flow. *Proc. R. Soc. A* **475**: 20190318.
http://dx.doi.org/10.1098/rspa.2019.0318

Received: 22 May 2019
Accepted: 18 September 2019

Subject Areas:
fluid mechanics, geophysics, mathematical modelling

Keywords:
bed particle saltation, turbulent wall-shear flow, bedload transport

Authors for correspondence
Ellora Padhi
e-mail: ellora@iitkgp.ac.in
Sk Zeeshan Ali
e-mail: skzeeshanali@iitkgp.ac.in
Subhasish Dey
e-mail: sdey@iitkgp.ac.in

Mechanics of bed particle saltation in turbulent wall-shear flow

Ellora Padhi[1], Sk Zeeshan Ali[1] and Subhasish Dey[1,2,3]

[1]Department of Civil Engineering, Indian Institute of Technology Kharagpur, West Bengal 721302, India
[2]Physics and Applied Mathematics Unit, Indian Statistical Institute Kolkata, West Bengal 700108, India
[3]Department of Hydraulic Engineering, State Key Laboratory of Hydro-Science and Engineering, Tsinghua University, Beijing 100084, People's Republic of China

EP, 0000-0002-2295-2171; SZA, 0000-0003-0763-7437; SD, 0000-0001-9764-1346

In this paper, we explore the mechanics of bed particle saltation in turbulent wall-shear flow, analysing the forces on a particle to perform saltation. The hydrodynamic drag encompasses the form drag and turbulent drag. The hydrodynamic lift comprises the Saffman lift, Magnus lift and turbulent lift. The subtle role of the Basset force in governing the particle trajectory is accounted for in the analysis. The bedload flux, emanating from the mathematical analysis of bed particle saltation, is determined. The results reveal that for the particle parameter range 20–100, the transport stage function equalling unity corroborates the threshold of bed particle saltation, where the saltation height and length are 1.3 and 9 times the particle size. For a given transport stage function, the relative saltation height and length decrease with an increase in particle parameter. For the particle parameter range 20–100, the relative saltation height and length increase with an increase in transport stage function, reaching their peaks, and then, they decrease. For a given particle parameter, the peak and mean particle densimetric Froude numbers increase as the transport stage function increases. The bedload flux curves for particle parameters 26 and 63 produce the upper and lower bound curves, respectively.

THE ROYAL SOCIETY PUBLISHING

1. Introduction

The bed particle saltation driven by a turbulent wall-shear flow over a sediment bed fascinates researchers. A good understanding of this phenomenon is a central requirement in multifarious engineering and industrial applications; for instance, in predicting the sand flux in a desert, the sedimentary patterns in a subaqueous environment and many others. Despite a plethora of studies over the decades, the mechanics of bed particle saltation remains inadequately understood, as most of the studies on the topic overlie empirical foundation. It turns out that a promising theoretical analysis that embraces the essential physical mechanisms of bed particle saltation is far from complete.

In a recent review article, Ali & Dey [1] provided a state-of-the-science of bed particle saltation in turbulent wall shear flow, scrutinizing the salient features of bed particle saltation in the light of experimental, theoretical and numerical frameworks (for details, see the references therein). In essence, the computational fluid dynamics schemes have provided an enhanced understanding of the mutual interplay between the near-bed coherent structures and the bed particle motion [2–5]. A wide variety of numerical techniques have been applied by researchers to examine the particle dynamics; for instance, the direct numerical simulation (DNS) together with the immersed boundary method (IBM) [6], the combined DNS, IBM and finite-discrete element method [3,7], and the large eddy simulation in conjunction with the discrete element model (DEM) [8,9].

Ali & Dey [1] specifically emphasized that although impressive advances have been made on the topic principally on experimental and numerical grounds, an exclusive theoretical analysis in exploring the mechanics of bed particle saltation requires further attention. To this end, researchers need to seek a generalized force system that would be able to accomplish the key mechanism of the fluid–particle interaction. Although Ali & Dey [1] put forward explicitly the current challenges in modelling of bed particle saltation from a broader perspective, here we put into focus the major limitations of the existing mathematical models. These are succinctly furnished below.

— In several studies, the hydrodynamic drag and lift on a particle to perform a saltation were considered based on the time-averaged flow assumptions [10–16]. In consequence, the mathematical models lack the crucial effects of velocity fluctuations, whose importance is worth considering for natural flows.
— The hydrodynamic drag was treated solely as a function of dynamic pressure by introducing a drag coefficient. The delicate role of the streamwise advective acceleration, giving rise to a turbulent drag, was completely overlooked [10–17].
— Researchers considered the hydrodynamic lift as sum of the Saffman lift and Magnus lift. The former results from a steep velocity gradient in the wall-shear layer, while the latter originates due to a spinning motion of the particle. However, the effects of normal advective acceleration that could induce a turbulent lift were disregarded in the theoretical analysis [10,13–16].
— To model the Saffman lift and Magnus lift, the mathematical models usually employ a so-called lift coefficient, whose physical significance is rather fuzzy. This is because of the fact that unlike the drag coefficient, no generic consensus has so far been realized regarding the precise measure of the lift coefficient [18]. Importantly, the artful use of a lift coefficient in the mathematical models helps to obtain a satisfactory matching of the analytical results with the experimental data. This is accredited to the fact that the lift coefficient is either assigned as a constant value or calibrated with the experimental data for fine-tuning the model results regardless of how weird the magnitude of hydrodynamic lift might be [10]. Therefore, such an analytical artifice leads to an unexpected estimation of the total hydrodynamic lift, which becomes several orders of magnitude as compared to the calculated Saffman lift and Magnus lift using their well-established lift coefficients.

— The Basset force, excepting a few studies, was in general overlooked with regard to sediment transport problems [10–12,14,17]. Besides, in some cases, although the Basset force term was included, its solution was unexpectedly simplified [13,19]. However, its inclusion and appropriate solution in the mathematical analysis in conjunction with the turbulent drag and turbulent lift are still lacking.

Estimation of the characteristic features of bed particle saltation, such as the particle trajectory, saltation height, saltation length and particle velocity has been the primary goal of analytical studies [1]. To fulfil this target, the bottom line is to solve the Lagrangian equations of motion of a particle performing a saltation [20–22]. For simplicity, the particle trajectory is sought in a two-dimensional frame. The turbulent wall-shear flow acts as a motivating agent to detach the particles from the sediment bed. This can happen when the fluid-induced applied bed shear stress exceeds its threshold value in lifting mode to set the particles to perform brief jumps in succession [18]. The boundary conditions accompanying the governing equations are carefully set based on the experimental observations. Additionally, the estimation of particle flux remains a subject of major interest to researchers [23,24]. In essence, with regard to a subaqueous environment, bed particle saltation contributes predominantly to the bedload transport [18,25,26]. The bedload flux can be estimated by extending the mathematical analysis of bed particle saltation [10,12,16].

Given the above overview, this study aims at exploring the mechanics of bed particle saltation in a subaqueous turbulent wall-shear flow. We specifically put into focus the fluid–particle interaction that is subtler than the particle–particle interaction. It turns out that the probability of particle collisions above the sediment bed is considered to be minimal in order to simplify the equations of random particle motion. The set of governing equations considering an improved force system is solved to explore the characteristic features of bed particle saltation. Then, the bedload flux is estimated by projecting the mathematical analysis of bed particle saltation. Keeping in mind a rich state-of-the-science of the subject, this study not only provides an improvement of the aforementioned limitations of the existing mathematical models but also builds a promising agreement between theory and practice.

The paper is organized as follows. In §2, the theoretical analysis of bed particle saltation is presented, including the description of the physical system, force system, velocity and turbulence intensity laws. The computational results of the particle trajectory, saltation height, saltation length, particle velocity and bedload flux are furnished in §3. Finally, the conclusion is drawn in §4.

2. Theoretical analysis

(a) Description of physical system

The physical system describes an incompressible turbulent fluid flow over a loosely packed sediment bed from where sediment particles are momentarily lifted off the bed performing series of brief jumps, called saltation (figure 1). The approach flow is featured by a turbulent wall-shear flow, encompassing a wide spectrum of *friction Reynolds number* $\mathscr{R}$ (also see table 1). The friction Reynolds number $\mathscr{R}$ is defined as [18]

$$\mathscr{R} = \frac{u_* k_s}{\nu}, \tag{2.1}$$

where u_* is the friction velocity $[= (\tau_b/\rho_f)^{1/2}]$, τ_b is the applied bed shear stress, ρ_f is the mass density of fluid, k_s is the roughness height, often called *Nikuradse equivalent sand roughness* and ν is the coefficient of kinematic viscosity of fluid. The roughness height k_s is conventionally expressed as a multiplier of bed particle size d as $k_s = \beta d$, where β is the proportionality constant [27]. However, for uniform sediment particles, β is approximately unity. In equation (2.1), the friction Reynolds number $\mathscr{R}$ characterizes the importance of fluid inertia relative to viscous damping. It is used to distinguish various flow regimes in a turbulent wall-shear flow; for instance, hydraulically smooth ($\mathscr{R} \leq 5$), transitional ($5 < \mathscr{R} < 70$) and rough ($\mathscr{R} \geq 70$) flow regimes. In

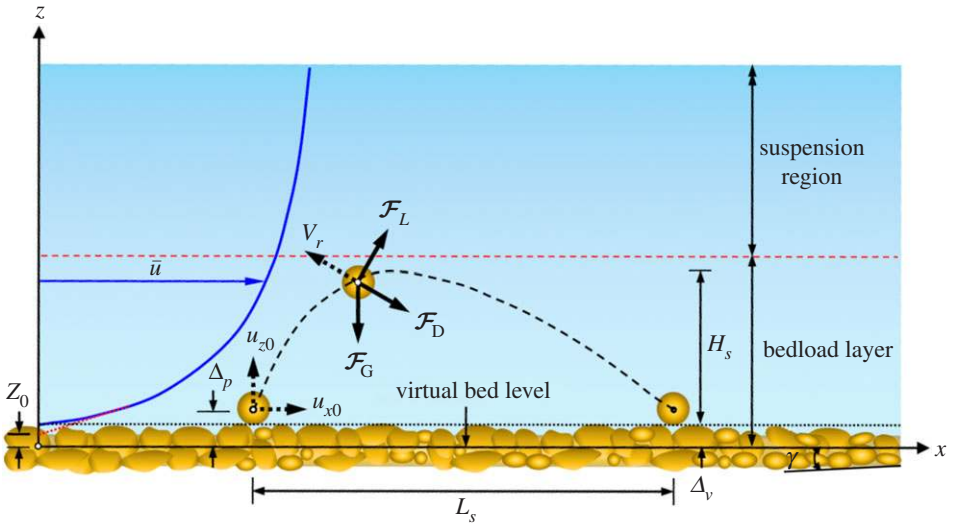

Figure 1. Conceptual sketch of bed particle saltation in turbulent wall-shear flow.

Table 1. Nomenclature.

C_D	drag coefficient
C_v	volumetric particle concentration within bedload layer
C_0	peak bedload concentration
c_m	added mass coefficient
$\mathscr{D}$	particle parameter
d	particle size
F_B	Basset force
$\mathcal{F}_{Bx}$, $\mathcal{F}_{Bz}$	components of the Basset force in (x, z)
$\mathcal{F}_D$	hydrodynamic drag
$\mathcal{F}_{DF}$	form drag
$\mathcal{F}_{DT}$	turbulent drag
F_d	particle densimetric Froude number
F_{dm}	mean particle densimetric Froude number
F_{ds}	peak particle densimetric Froude number
$\mathcal{F}_G$	submerged weight of particle
$\mathcal{F}_L$	hydrodynamic lift
$\mathcal{F}_{LM}$	Magnus lift
$\mathcal{F}_{LS}$	Saffman lift
$\mathcal{F}_{LT}$	turbulent lift
g	gravitational acceleration
H_s	saltation height

(*Continued*.)

Table 1. (*Continued.*)

h	flow depth
k_s	roughness height
L_s	saltation length
M_T	total mass of particle including added fluid mass
P_S	particle entrainment probability in a saltating mode
$\bar{p}$	time-averaged pressure intensity
Q_b	bedload flux in volume per unit time and bed width
$\mathscr{R}$	friction Reynolds number
$\mathscr{R}_p$	particle Reynolds number
T	transport stage function
t	time
t_0	initial time
u_*	friction velocity
u_{*c}	threshold friction velocity
u_{fx}, u_{fz}	instantaneous flow velocity components in (x, z)
$\bar{u}_{fx}, \bar{u}_{fz}$	time-averaged flow velocity components in (x, z)
u'_{fx}, u'_{fz}	fluctuations of (u_{fx}, u_{fz}) from their time-averaged values
u_{ps}	streamwise particle velocity at saltation peak
$\bar{u}_{px}, \bar{u}_{pz}$	components of particle velocity in (x, z)
$\bar{u}_{x0}, \bar{u}_{z0}$	initial particle velocity components in (x, z)
V_p	mean particle velocity
V_r	particle velocity relative to fluid flow
V_{rm}	mean particle relative velocity
W	elementary width across the particle
x, z	Cartesian coordinates
z_0	zero-velocity level
α_L	Saffman lift coefficient
β	proportionality constant
Δ_v	distance between virtual bed level and crest of bed particles
Δ_p	initial position of a saltating particle from virtual bed level
ε	turbulent kinetic energy dissipation rate
Φ_b	bedload flux function
γ	streamwise inclination of virtual bed level with horizontal
ϑ	dummy variable
κ	von Kármán coefficient
λ	Taylor microscale
ν	coefficient of kinematic viscosity of fluid
Θ	Shields number

(*Continued*.)

Table 1. (*Continued.*)

Θ_c	threshold Shields number
ρ_f	mass density of fluid
ρ_p	mass density of particles
σ_x, σ_z	turbulence intensity components in (x, z)
τ_b	applied bed shear stress
τ_{bc}	threshold bed shear stress
Ω_m	maximum angular velocity of particle
Ψ_b	flow intensity function

essence, for a mobile-bed flow, the applied bed shear stress τ_b surpasses the threshold bed shear stress τ_{bc}, giving rise to various kinds of particle transport. The surplus bed shear stress $\tau_b - \tau_{bc}$ driving the particle transport is expressed in dimensionless form by introducing the *transport stage function* T. It is defined as

$$T = \frac{\Theta - \Theta_c}{\Theta_c} \quad \text{and} \quad \Theta = \frac{\rho_f u_*^2}{(\rho_p - \rho_f) g d}, \tag{2.2}$$

where Θ is the Shields number, Θ_c is the threshold Shields number, i.e. $\Theta_c = \Theta(u_* = u_{*c})$, where u_{*c} is the threshold friction velocity $[= (\tau_{bc}/\rho_f)^{1/2}]$, ρ_p is the mass density of particles and g is the gravitational acceleration. In particular, when the Shields number Θ just exceeds its threshold value Θ_c, the particles exhibit rolling and/or sliding motion in contact with the sediment bed. Accurate determination of the threshold Shields number Θ_c requires an in-depth analysis of the typical force system on a target sediment particle [27,28]. To envision the behaviour of the threshold Shields number Θ_c in various flow regimes, we introduce the *particle parameter* $\mathscr{D}$, which measures the importance of gravity force relative to viscous force. The particle parameter $\mathscr{D}$ is expressed as

$$\mathscr{D} = \left[\frac{g d^3}{\nu^2} \left(\frac{\rho_p}{\rho_f} - 1 \right) \right]^{1/3}. \tag{2.3}$$

In this study, a set of empirical expressions for the threshold Shields number Θ_c given by Cao *et al*. [29] is considered. It is expressed as

$$\Theta_c(\mathscr{D} \le 3.52) = 0.141 \mathscr{D}^{-0.345}, \Theta_c(3.52 < \mathscr{D} < 43.1) = 0.324 \mathscr{D}^{-1.02} \left(1 + 1.96 \times 10^{-5} \mathscr{D}^{4.26}\right)^{0.35}$$
$$\text{and} \qquad \Theta_c(\mathscr{D} \ge 43.1) = 0.045. \tag{2.4}$$

As the Shields number Θ increases further, the particles are transported in a saltating mode (figure 1), as considered here. The bed particle saltation is essentially restricted to a thin fluid layer, called *bedload layer*, as illustrated in figure 1. For large values of Shields number Θ, the finer bed particles principally belong to the *suspension region* that exists beyond the bedload layer (figure 1). However, in this study, we focus specifically into the mechanism of bed particle saltation.

With reference to a Cartesian coordinate system (x, z) as depicted in figure 1, we consider the virtual bed level $(z = 0)$ at a distance of Δ_v below the crest of bed particles. The streamwise inclination of the virtual bed level with the horizontal is denoted by γ. In addition, the initial position of a saltating particle is considered at $z = \Delta_p$. The distance between the particle centroid at the topmost position of the particle trajectory and the crest level, called *saltation height*, is represented by H_s. Furthermore, the streamwise distance covered by a saltating particle during a saltation step, called *saltation length*, is denoted by L_s. The initial particle velocity components in (x, z) are denoted by (u_{x0}, u_{z0}).

(b) Force system

The set of equations representing the trajectory of a saltating particle in xz-plane reads [1]

$$M_T \frac{\mathrm{d}u_{px}}{\mathrm{d}t} = \mathcal{F}_G \sin\gamma + \mathcal{F}_D\left(\frac{\bar{u}_{fx} - u_{px}}{V_r}\right) + \mathcal{F}_L\left(\frac{u_{pz}}{V_r}\right) + \mathcal{F}_{Bx}, \tag{2.5a}$$

$$M_T \frac{\mathrm{d}u_{pz}}{\mathrm{d}t} = -\mathcal{F}_G \cos\gamma - \mathcal{F}_D\left(\frac{u_{pz}}{V_r}\right) + \mathcal{F}_L\left(\frac{\bar{u}_{fx} - u_{px}}{V_r}\right) - \mathcal{F}_{Bz}, \tag{2.5b}$$

$$\frac{\mathrm{d}x}{\mathrm{d}t} = u_{px} \tag{2.5c}$$

and

$$\frac{\mathrm{d}z}{\mathrm{d}t} = u_{pz}, \tag{2.5d}$$

where M_T is the total mass of the particle including the *added fluid mass*, t is the time, (u_{px}, u_{pz}) are the components of particle velocity in (x, z), $\mathcal{F}_G$ is the submerged weight of the particle, $\mathcal{F}_D$ is the hydrodynamic drag, $\bar{u}_{fx}$ is the time-averaged streamwise flow velocity, V_r is the particle velocity relative to the fluid flow, i.e. $[(\bar{u}_{fx} - u_{px})^2 + u_{pz}^2]^{1/2}$, $\mathcal{F}_L$ is the hydrodynamic lift and $(\mathcal{F}_{Bx}, \mathcal{F}_{Bz})$ are the components of the Basset force $\mathbf{F}_B$ in (x, z).

The total particle mass M_T is expressed as

$$M_T = \frac{1}{6}(\rho_p + c_m\rho_f)\pi d^3, \tag{2.6}$$

where c_m is the added mass coefficient. The introduction of the added mass coefficient c_m to the physical system is pertinent here, because an accelerating or a retarding particle in a fluid moves a specific volume of contiguous fluid. Since both the fluid and particle cannot possess the same space simultaneously, we consider a specific volume of fluid to be in motion with the particle. In this study, $c_m = 0.5$ is considered [10].

The submerged weight $\mathcal{F}_G$ of the particle is expressed as

$$\mathcal{F}_G = \frac{\pi d^3}{6}(\rho_p - \rho_f)g. \tag{2.7}$$

It is worth highlighting that in the theoretical analysis, we have considered the critical case, where the contributions from all the forces to the particle motion are taken into account. This is indeed likely from the perspective of preventive measures against erosion. The hydrodynamic drag $\mathcal{F}_D$ consists of the form drag $\mathcal{F}_{DF}$ and the turbulent drag $\mathcal{F}_{DT}$. In fact, the classical system is unable to describe all the essential components of hydrodynamic drag acting on a sediment particle, even at the entrainment, in a turbulent wall-shear flow. Therefore, in this study, we split the hydrodynamic drag into form drag and turbulent drag, as was considered recently by Ali & Dey [30]. An in-depth analysis of the orders of magnitude of form drag and turbulent drag was also performed by Ali & Dey [30]. This has provided an idea of the relative contribution from the hydrodynamic drag to the system of governing equations (2.5*a*)–(2.5*d*). Thus, considering the appropriate directions, the hydrodynamic drag $\mathcal{F}_D$ appearing in equations (2.5*a*) and (2.5*b*), respectively, is expressed as

$$\mathcal{F}_D = \mathcal{F}_{DF} + \mathcal{F}_{DT}\left(\frac{V_r}{\bar{u}_{fx} - u_{px}}\right) \quad \text{and} \quad \mathcal{F}_D = \mathcal{F}_{DF} + \mathcal{F}_{DT}\left(\frac{V_r}{u_{pz}}\right). \tag{2.8}$$

The form drag $\mathcal{F}_{DF}$ on a particle results from the pressure and viscous skin friction. It is traditionally expressed as a function of dynamic pressure. Therefore, the form drag $\mathcal{F}_{DF}$ reads

$$\mathcal{F}_{DF} = C_D\frac{1}{2}\rho_f V_r^2\frac{\pi d^2}{4}, \tag{2.9}$$

where C_D is the drag coefficient. In this study, the drag coefficient C_D for spherical particles, given by Yen [31] is considered. It is

$$C_D = \frac{24}{\mathscr{R}_p}(1 + 0.15\mathscr{R}_p^{1/2} + 0.017\mathscr{R}_p) - \frac{0.208}{1 + 10^4\mathscr{R}_p^{-1/2}}, \tag{2.10}$$

where $\mathscr{R}_p$ is the particle Reynolds number ($=\mid V_r \mid d/\nu$). The above equation is valid over a wide spectrum of particle Reynolds number, as suggested by Niño & García [15].

The turbulent drag $\mathcal{F}_{DT}$ on a particle arises from significant streamwise pressure gradient. The turbulent drag $\mathcal{F}_{DT}$ is expressed as follows [30]:

$$\mathcal{F}_{DT} = -\left(\frac{\partial \bar{p}}{\partial x}\right) W\frac{\pi d^2}{4}, \tag{2.11}$$

where $\bar{p}$ is the time-averaged pressure intensity and W is the elementary width across the particle ($= d$ for a saltating particle).

The time-averaged pressure gradients in (x, z) can be obtained from the Euler equations as

$$-\frac{\partial \bar{p}}{\partial x} = \rho_f \overline{\frac{\mathrm{D}u_{fx}}{\mathrm{D}t}} \tag{2.12a}$$

and

$$-\frac{\partial \bar{p}}{\partial z} = \rho_f \overline{\frac{\mathrm{D}u_{fz}}{\mathrm{D}t}}, \tag{2.12b}$$

where (u_{fx}, u_{fz}) are the instantaneous flow velocity components in (x, z) and $(\mathrm{D}u_{fx}/\mathrm{D}t,\ \mathrm{D}u_{fz}/\mathrm{D}t)$ are the total acceleration components in (x, z). In the above equations, we have considered that the pressure gradient terms are free from the viscous effects to simplify the mathematical treatment. Following the Reynolds decomposition [18], u_{fx} and u_{fz} are expressed as $u_{fx} = \bar{u}_{fx} + u'_{fx}$ and $u_{fz} = \bar{u}_{fz} + u'_{fz}$, respectively, where $\bar{u}_{fz}$ is the time-averaged normal flow velocity and (u'_{fx}, u'_{fz}) are the fluctuations of (u_{fx}, u_{fz}) from their time-averaged values. A steady-state condition produces $\mathrm{D}u_{fx}/\mathrm{D}t = u_{fx}(\partial u_{fx}/\partial x) + u_{fz}(\partial u_{fx}/\partial z)$ and $\mathrm{D}u_{fz}/\mathrm{D}t = u_{fx}(\partial u_{fz}/\partial x) + u_{fz}(\partial u_{fz}/\partial z)$. For a unidirectional streamflow, $\bar{u}_{fx} = \bar{u}_{fx}(z)$, $\bar{u}_{fz} = 0$ and $\partial \bar{u}_{fx}/\partial x = 0$. Therefore, performing the time-averaging of the total acceleration components in (x, z) yields

$$\overline{\frac{\mathrm{D}u_{fx}}{\mathrm{D}t}} = \sqrt{\overline{u'^2_{fx}}}\sqrt{\overline{\left(\frac{\partial u'_{fx}}{\partial x}\right)^2}} + \sqrt{\overline{u'^2_{fz}}}\sqrt{\overline{\left(\frac{\partial u'_{fx}}{\partial z}\right)^2}} \tag{2.13a}$$

and

$$\overline{\frac{\mathrm{D}u_{fz}}{\mathrm{D}t}} = \sqrt{\overline{u'^2_{fx}}}\sqrt{\overline{\left(\frac{\partial u'_{fz}}{\partial x}\right)^2}} + \sqrt{\overline{u'^2_{fz}}}\sqrt{\overline{\left(\frac{\partial u'_{fz}}{\partial z}\right)^2}}, \tag{2.13b}$$

where the over-bar denotes the time-averaging. By means of the statistical theory of turbulence, following relationships can be obtained [28,30]:

$$\overline{\left(\frac{\partial u'_{fx}}{\partial x}\right)^2} = \frac{\overline{u'^2_{fx}}}{\lambda^2}, \quad \overline{\left(\frac{\partial u'_{fx}}{\partial z}\right)^2} = \frac{2\overline{u'^2_{fx}}}{\lambda^2} + \frac{1}{4\overline{u'^2_{fx}}}\left(\frac{\partial \overline{u'^2_{fx}}}{\partial z}\right)^2 \quad \text{and} \quad \overline{\left(\frac{\partial u'_{fz}}{\partial x}\right)^2} = \frac{2\overline{u'^2_{fz}}}{\lambda^2}, \tag{2.14}$$

where λ is the Taylor microscale. Substituting equation (2.14) into equations (2.13*a*) and (2.13*b*) yields

$$\overline{\frac{\mathrm{D}u_{fx}}{\mathrm{D}t}} = \frac{\sigma_x^2}{\lambda} + \sigma_z\left[2\frac{\sigma_x^2}{\lambda^2} + \frac{1}{4\sigma_x^2}\left(\frac{\partial \sigma_x^2}{\partial z}\right)^2\right]^{1/2} \tag{2.15a}$$

and

$$\frac{\overline{\mathrm{D}u_{fz}}}{\mathrm{D}t} = \frac{\sqrt{2}\sigma_x\sigma_z}{\lambda} + \frac{1}{2}\frac{\partial\sigma_z^2}{\partial z}, \tag{2.15b}$$

where (σ_x, σ_z) are the turbulence intensity components, i.e. $[(\overline{u_{fx}'^2})^{1/2}, (\overline{u_{fz}'^2})^{1/2}]$ in (x, z).

The Taylor microscale λ appearing in equation (2.15) can be expressed as follows [32]:

$$\lambda = \left(15\nu\frac{\sigma_x^2}{\varepsilon}\right)^{1/2}, \tag{2.16}$$

where ε is the turbulent kinetic energy dissipation rate. It is expressed as follows [33]:

$$\varepsilon = 0.691\frac{\sigma_x^3}{(zh)^{1/2}}, \tag{2.17}$$

where h is the flow depth.

The hydrodynamic lift $\mathcal{F}_L$ on a particle comprises of *Saffman lift* $\mathcal{F}_{LS}$, *Magnus lift* $\mathcal{F}_{LM}$ and *turbulent lift* $\mathcal{F}_{LT}$. An in-depth analysis of the orders of magnitude of Saffman lift, Magnus lift and turbulent lift was performed by Ali & Dey [30]. This has provided an idea of the relative contribution from the hydrodynamic lift to the system of governing equations (2.5*a*)–(2.5*d*). Thus, considering the appropriate directions, the hydrodynamic lift $\mathcal{F}_L$ appearing in equations (2.5*a*) and (2.5*b*), respectively, is expressed as

$$\mathcal{F}_L = \mathcal{F}_{LS} + \mathcal{F}_{LM} + \mathcal{F}_{LT}\left(\frac{V_r}{u_{pz}}\right) \quad \text{and} \quad \mathcal{F}_L = \mathcal{F}_{LS} + \mathcal{F}_{LM} + \mathcal{F}_{LT}\left(\frac{V_r}{\bar{u}_{fx} - u_{px}}\right). \tag{2.18}$$

The *Saffman lift* $\mathcal{F}_{LS}$ on a particle arises owing to a steep velocity gradient $\partial\bar{u}_{fx}/\partial z$ in the wall-shear layer. The $\mathcal{F}_{LS}$ is expressed as follows [34,35]:

$$\mathcal{F}_{LS} = \alpha_L\rho_f\nu^{1/2}V_r d^2\left(\frac{\partial\bar{u}_{fx}}{\partial z}\right)^{1/2}, \tag{2.19}$$

where α_L is the Saffman lift coefficient ($= 1.615$).

The *Magnus lift* $\mathcal{F}_{LM}$ on a particle occurs owing to a rotational motion of the particle. The $\mathcal{F}_{LM}$ is expressed as follows [36]:

$$\mathcal{F}_{LM} = \frac{\pi}{8}\rho_f V_r d^3\Omega_m, \tag{2.20}$$

where Ω_m is the maximum angular velocity of the particle. In the above, the maximum angular velocity was considered in order to obtain the maximum Magnus lift on the particle. In this study, we consider $\Omega_m = 0.5\partial\bar{u}_{fx}/\partial z$ [36].

The *turbulent lift* $\mathcal{F}_{LT}$ on a particle arises from significant normal pressure gradient. It can be fairly linked with the total acceleration component in the normal direction. The $\mathcal{F}_{LT}$ for an exposed particle is expressed as follows [30]:

$$\mathcal{F}_{LT} = -\left(\frac{\partial\bar{p}}{\partial z}\right)d\left(\frac{\pi}{4}W^2\right) = \rho_f\left(\frac{\overline{\mathrm{D}u_{fz}}}{\mathrm{D}t}\right)\frac{\pi}{4}d^3. \tag{2.21}$$

In the above, the time-averaged total acceleration component in the normal direction is obtained from equation (2.15*b*).

In addition, the Basset force $\mathbf{F}_B$ on a particle arises owing to a change in the relative velocity of the particle with respect to fluid. It addresses the temporal delay in the boundary layer development adjoining the surface of the particle. The $\mathbf{F}_B$ is expressed as follows [1]:

$$\mathbf{F}_B = \frac{3}{2}\pi^{1/2}\rho_f\nu^{1/2}d^2\int_0^t\frac{\mathrm{d}\mathbf{V}_r}{\mathrm{d}\vartheta}\frac{\mathrm{d}\vartheta}{(t-\vartheta)^{1/2}} \approx \frac{3}{2}\pi^{1/2}\rho_f\nu^{1/2}d^2\sum_{i=1}^{n}\frac{\mathrm{d}\mathbf{V}_r}{(t_i - t_0)^{1/2}}, \tag{2.22}$$

where $\mathbf{V}_r$ is the relative velocity vector, ϑ is the dummy variable and t_0 is the initial time.

(c) Velocity and turbulence intensity laws

To solve the physical system, the flow velocity field needs to be properly defined over the spatial domain. Within the wall-shear layer, the streamwise flow velocity $\bar{u}_{fx}$ follows the classical logarithmic law. It is

$$\bar{u}_{fx} = \frac{u_*}{\kappa} \ln \frac{z}{z_0}, \tag{2.23}$$

where κ is the von Kármán coefficient and z_0 is the zero-velocity level (figure 1). The zero-velocity level z_0 is expressed as follows [18]:

$$z_0(\mathscr{R} \le 5) = 0.11 \frac{\nu}{u_*}, \quad z_0(5 < \mathscr{R} < 70) = 0.11 \frac{\nu}{u_*} + \frac{k_s}{30} \quad \text{and} \quad z_0(\mathscr{R} \ge 70) = \frac{k_s}{30}. \tag{2.24}$$

In a turbulent wall-shear flow, the streamwise turbulence intensity σ_x can be obtained using the expression given by Nezu [37]. It is expressed as

$$\sigma_x = 2.3 u_* \exp\left(-\frac{z}{h}\right). \tag{2.25}$$

In addition, the normal turbulence intensity σ_z is expressed as follows [38]:

$$\sigma_z = 0.5 \sigma_x. \tag{2.26}$$

3. Computational results and discussion

The set of ordinary differential equations [see equations (2.5*a*)–(2.5*d*)] can be readily solved numerically for a set of characteristic parameters. The time step for the numerical solution was taken as 10^{-4} s. The virtual bed level is considered at a distance of $d/4$ below the crest of bed particles, i.e. $\Delta_v = 0.25d$ [10]. In addition, following the experimental results of Abbott & Francis [39], the boundary conditions associated with equations (2.5*a*)–(2.5*d*) are expressed as follows:

$$x|_{t=0} = 0, \quad z|_{t=0} = \Delta_p = 0.6d, \quad u_{x0} = u_{px}\big|_{t=0} = 2.5u_* \quad \text{and} \quad u_{z0} = u_{pz}\big|_{t=0} = 2.5u_*. \tag{3.1}$$

Here, we first present the particle trajectory, saltation height, saltation length and particle velocity obtained from this study and then, the estimation of bedload flux, stemming from the theoretical analysis of bed particle saltation.

(a) Particle trajectory, saltation height and saltation length

Figure 2*a–c* depicts the comparison of the bed particle saltation trajectories obtained from this study with the experimental data. The particle saltation trajectories are represented by plotting the relative streamwise distance x/d as a function of relative normal distance z/d. The experimental data of Lee & Hsu [14] and Niño & García [15,40] include particle sizes of $d = 1.36$, 0.67 and 0.56 mm. In general, the comparison of the computed particle saltation trajectories with the experimental data is quite satisfactory. This reveals that the consideration of the hydrodynamic force system of this study is capable to predict the trajectories of bed particle saltation as observed in the laboratory measurements. In essence, it was found that the consideration of the turbulent drag and the turbulent lift in this study provided an improved matching of the computed particle saltation trajectories with the experimental data compared with those obtained by Niño & García [15]. The reason is that Niño & García [15] did not consider the subtle effects of the turbulent drag and the turbulent lift. It turns out that in order to predict the particle saltation trajectories precisely, the turbulent drag and lift need to be included in the theoretical analysis, as is done in this study. It is pertinent to mention that the characteristic parameters of a particle saltation trajectory are the saltation height, saltation length and particle velocity. These features are described subsequently.

Figure 3 shows the relative saltation height H_s/d as a function of transport stage function T for different values of particle parameter $\mathscr{D}(= 10, 20, 30, 40, 50, 60, 70, 80$ and $100)$. To prepare figure 3 and subsequent computed curves, we consider the mass densities of particle and fluid as $\rho_p = 2650\,\mathrm{kg\,m^{-3}}$ and $\rho_f = 1000\,\mathrm{kg\,m^{-3}}$, respectively, and flow depth $h = 30d$. It appears that

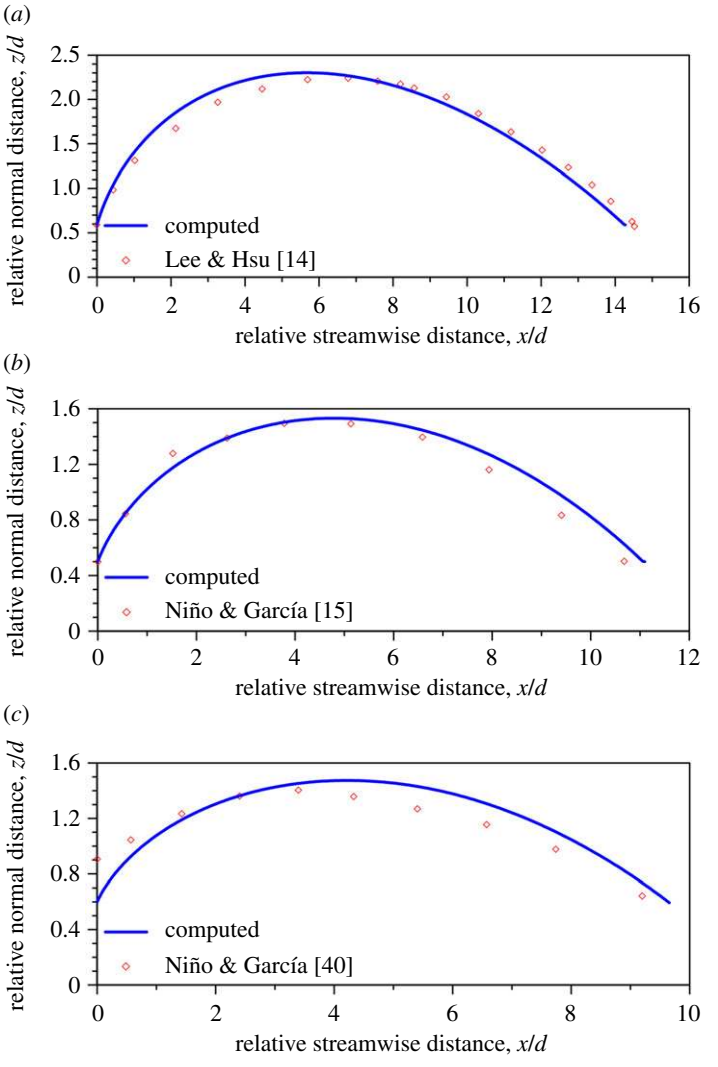

Figure 2. Comparison of the bed particle trajectories obtained from this study with the experimental data for (*a*) $d = 1.36$ mm, (*b*) $d = 0.67$ mm and (*c*) $d = 0.56$ mm. (Online version in colour.)

for a given transport stage function, the relative saltation height decreases with an increase in particle parameter. This observation is in conformity with the reality, because for a given applied bed shear stress, a finer particle attains a higher saltation height than a coarser particle [41,42]. In addition, figure 3 indicates that for a given particle parameter as $\mathscr{D} = 10$, the relative saltation height increases as the transport stage function increases. However, for a given particle parameter ($\mathscr{D} > 10$), the relative saltation height initially increases with an increase in transport stage function, reaching its peak and then, it reduces gradually with a further increase in transport stage function. The reduction in the relative saltation height with an increase in transport stage function is primarily attributed to the deceleration effects [14]. Moreover, it is noticeable that the peak saltation height is achieved earlier for larger values of particle parameter.

It is interesting to shed light on the surplus bed shear stress (or the transport stage function T in dimensionless form) corresponding to the threshold of bed particle saltation. To this end, in figure 3, we note that for a transport stage function equalling unity ($T = 1$), the relative saltation height H_s/d essentially becomes independent of particle parameter $\mathscr{D}$ for $20 \leq \mathscr{D} \leq 100$

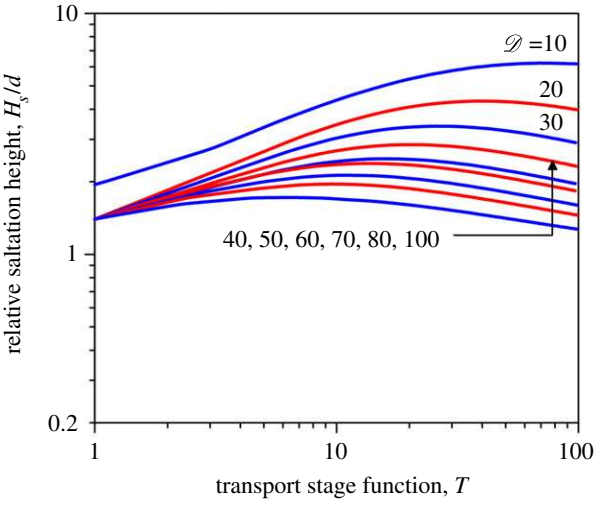

Figure 3. Relative saltation height H_s/d versus transport stage function T for different values of particle parameter $\mathscr{D}$. (Online version in colour.)

or equivalently for $0.79 \leq d \leq 3.95$ mm, as obtained from equation (2.3). A crucial question in this regard arises: what does this independency really signify? This question can be answered from the most fundamental tenet of the threshold of particle transport mechanism in various modes depending on the applied bed shear stress. The condition $T = 1$, in fact, suggests that the Shields number is twice its threshold value ($\Theta = 2\Theta_c$). From equation (2.4), the threshold Shields numbers Θ_c for $\mathscr{D} = 20$ and 100 are obtained as $\Theta_c = 0.031$ and 0.045, respectively. Furthermore, using equations (2.1)–(2.3), the friction Reynolds number $\mathscr{R}$ can be expressed as $\mathscr{R} = \Theta^{1/2}\mathscr{D}^{3/2}$. Therefore, the friction Reynolds numbers $\mathscr{R}$ corresponding to $\Theta_c = 0.031$ and 0.045 are obtained as $\mathscr{R} = 15.84$ (hydraulically transitional flow regime) and 212.13 (hydraulically rough flow regime), respectively. Importantly, in the range $15.84 \leq \mathscr{R} \leq 212.13$ (hydraulically transitional to rough flow regimes), it has been found that the condition $\Theta = 2\Theta_c$ is fairly close to the threshold of particle transport in a saltating mode for fully exposed particles [28]. Therefore, it transpires that the condition $T = 1$ corresponds to the threshold of bed particle saltation (also evident from figure 3). However, this estimation of the threshold of bed particle saltation is somewhat lower than that obtained from the empirical relationship [41], given by $P_S = 1 - 1.84T^{-0.94}$, where P_S is the particle entrainment probability in a saltating mode. This relationship predicts the transport stage function corresponding to the threshold of bed particle saltation to be $T(P_S \to 0) = 1.91$. This study shows that for $T = 1$, the relative saltation height for $20 \leq \mathscr{D} \leq 100$ becomes approximately as $H_s/d = 1.3$ (> 1). This also suggests the bed particle detachment threshold for which the bed particle is just capable to perform a saltation.

Figure 4 illustrates the comparison of the computed relative saltation height H_s/d with the experimental data. The experimental data of Abbott & Francis [39], Hu & Hui [43], Ancey *et al.* [44] and Ramesh *et al.* [45] are considered here. It appears that the computed values of relative saltation height have a satisfactory agreement with the experimental data.

Figure 5 furnishes the relative saltation length L_s/d as a function of transport stage function T for different values of particle parameter $\mathscr{D}$(=10, 20, 30, 40, 50, 60, 70, 80 and 100). It turns out that for a given transport stage function, the relative saltation length reduces with an increase in particle parameter. This is attributed to the fact that for a given applied bed shear stress, a finer particle achieves a longer saltation length as compared to a coarser particle. Akin to figures 3 and 5 also shows that for a given particle parameter as $\mathscr{D} = 10$, the relative saltation length increases with an increase in transport stage function. However, for a given particle parameter ($\mathscr{D} > 10$), the relative saltation length increases as the transport stage function increases, attaining its peak

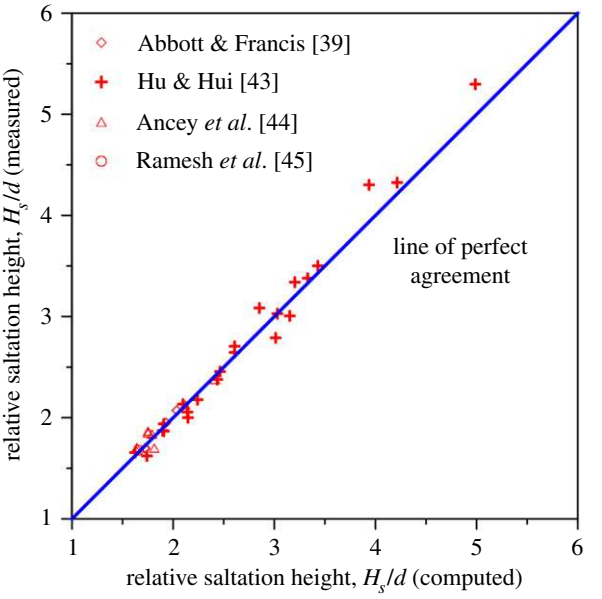

Figure 4. Computed versus measured relative saltation height H_s/d. (Online version in colour.)

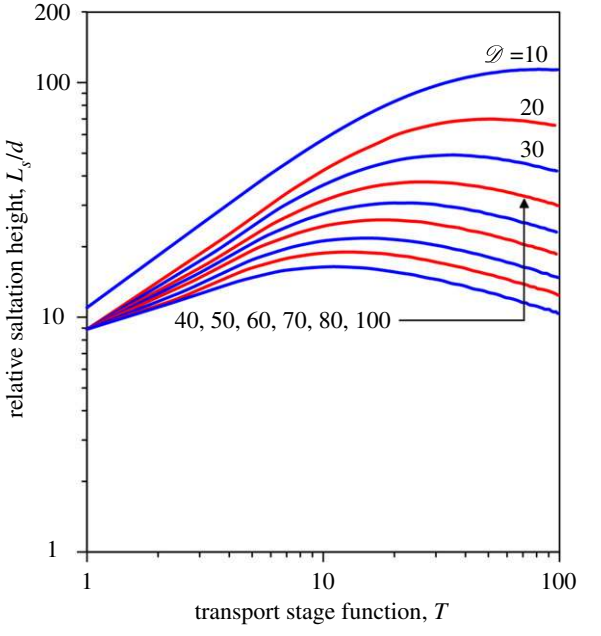

Figure 5. Relative saltation length L_s/d versus transport stage function T for different values of particle parameter $\mathscr{D}$. (Online version in colour.)

and thereafter, it decreases gradually with a further increase in transport stage function owing to the deceleration effects. Similar to figures 3 and 5 also provides the evidence of the threshold of bed particle saltation for $T = 1$ and $20 \leq \mathscr{D} \leq 100$. Furthermore, figure 5 indicates that for $T = 1$, the relative saltation length becomes approximately $L_s/d = 9$.

The validation of the computed relative saltation length L_s/d with the experimental data of Abbott & Francis [39], Hu & Hui [43], Ancey *et al*. [44] and Ramesh *et al*. [45] is presented in figure 6. In general, the computed values of relative saltation height have a good congruence

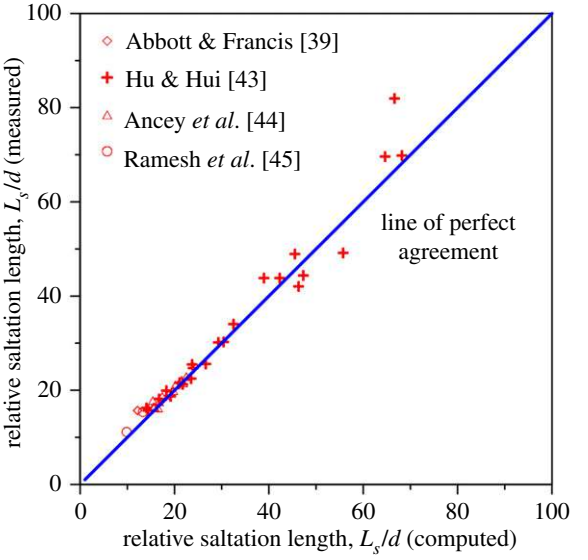

Figure 6. Computed versus measured relative saltation length L_s/d. (Online version in colour.)

with the experimental data. However, the computed relative saltation length departs from the experimental data of Hu & Hui [43] in the range $L_s/d > 60$.

In this context, it is worth highlighting that in previous mathematical models of bed particle saltation [10,12,17], for a given transport stage function, the relative saltation height and relative saltation length were surprisingly found to increase with an increase in particle parameter. These findings lack physical rationales and therefore they essentially contradict the experimental observations [41,46–49]. This is ascribed to the fact that for a given transport stage function, a finer particle achieves larger saltation height and saltation length as compared to a coarser particle for the same mass density. To be specific, a finer particle corresponds to a lighter mass than a coarser particle for the same mass density. The findings of this study are thus in plausible agreement with the reality.

(b) Particle velocity

We first intend to put into focus the streamwise particle velocity u_{px}. In dimensionless form, the streamwise particle velocity u_{px} can be expressed by introducing the *streamwise particle densimetric Froude number* F_d (henceforth *particle densimetric Froude number* for brevity). The F_d is expressed as $F_d = u_{px}/[(\rho_p/\rho_f - 1)gd]^{1/2}$. In order to grasp how the streamwise particle velocity varies with the surplus bed shear stress, we specifically consider the characteristic streamwise particle velocity u_{ps} at the saltation peak, i.e. $u_{ps} = u_{px}(z = H_s)$. Accordingly, the particle densimetric Froude number corresponding to the saltation peak, called *peak particle densimetric Froude number*, is expressed as $F_{ds} = u_{ps}/[(\rho_p/\rho_f - 1)gd]^{1/2}$. Figure 7 shows the peak particle densimetric Froude number F_{ds} as a function of transport stage function T for different values of particle parameter $\mathscr{D}(= 10, 20, 30, 40, 50, 60, 70, 80$ and $100)$. It is evident that for a given particle parameter, the peak particle densimetric Froude number increases as the transport stage function increases. However, it is revealed that for a given transport stage function, the peak particle densimetric Froude number varies insignificantly with the particle parameter for $\mathscr{D} > 10$. In fact, it appears that for the particle parameter range as $\mathscr{D} = 20$–100, the $F_{ds}(T)$ curves for different $\mathscr{D}$ form a thin band. To be specific, the $F_{ds}(T)$ curves for different $\mathscr{D}$ $(20 \leq \mathscr{D} \leq 100)$ are converging in nature in the range $1 \leq T \leq 2.2$, where at $T = 2.2$, the separation between the extremities of the thin band formed by the $F_{ds}(T)$ curves becomes a minimum. Interestingly, for $T = 30$ (or $\Theta = 31\Theta_c$), the $F_{ds}(T)$ curves for different $\mathscr{D}$ $(20 \leq \mathscr{D} \leq 100)$ become practically independent of $\mathscr{D}$ at $F_{ds} = 11.9$ (figure 7). In an

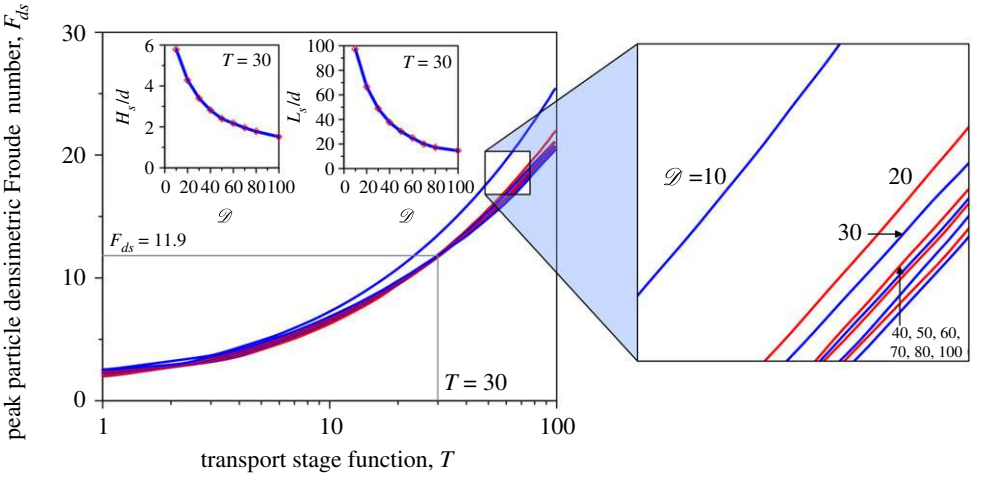

Figure 7. Peak particle densimetric Froude number F_{ds} versus transport stage function T for different values of particle parameter $\mathscr{D}$. In the inset, the variations of relative saltation height H_s/d and relative saltation length L_s/d with particle parameter $\mathscr{D}$ at a transport stage function T of 30 are shown. (Online version in colour.)

enlarged frame capturing the range of transport stage function as $46 \leq T \leq 82$, a clear picture of the $F_{ds}(T)$ curves for different $\mathscr{D}$ is depicted, since the curves are very close. The enlarged frame reveals that the peak particle densimetric Froude number reduces with an increase in particle parameter. Conversely, for $T < 30$, it has been found (not shown here by another enlarged frame) that the peak particle densimetric Froude number increases as the particle parameter increases. It turns out that $T = 30$ acts as a pivotal point, beyond which the $F_{ds}(T)$ curves for different $\mathscr{D}$ ($20 \leq \mathscr{D} \leq 100$) change their chronological trend with $\mathscr{D}$.

It is further interesting to shed light on the variations of the relative saltation height H_s/d and relative saltation length L_s/d with the particle parameter $\mathscr{D}$ at the pivotal point ($T = 30$). This is because of the fact that although at $T = 30$, the peak particle densimetric Froude numbers F_{ds} for different $\mathscr{D}$ ($20 \leq \mathscr{D} \leq 100$) remain invariant with $\mathscr{D}$, the H_s/d and L_s/d vary significantly with $\mathscr{D}$ at $T = 30$ (figures 3 and 5). Therefore, in the insets of figure 7, we show the $H_s/d(\mathscr{D})$ and $L_s/d(\mathscr{D})$ curves corresponding to $T = 30$. It appears that both the relative saltation height and relative saltation length decrease monotonically with an increase in particle parameter.

It is also interesting to shed light on the mean particle relative velocity V_{rm} during a saltation step. The V_{rm} can be obtained by averaging the particle velocity V_r relative to the fluid flow over a complete saltation step. In dimensionless form, the V_{rm} can be expressed by means of *mean particle densimetric Froude number* F_{dm} as $F_{dm} = V_{rm}/[(\rho_p/\rho_f - 1)gd]^{1/2}$. In figure 8, the mean particle densimetric Froude number F_{dm} as a function of transport stage function T for different values of particle parameter $\mathscr{D}$(= 10, 20, 30, 40, 50, 60, 70, 80 and 100) is shown. Clearly, for the particle parameter range as $\mathscr{D} = 20$–100, the $F_{dm}(T)$ curves for different $\mathscr{D}$ form a thin band. In an enlarged frame, a clear representation of the $F_{dm}(T)$ curves for different $\mathscr{D}$ is provided, because the curves are congested. For a given particle parameter, the mean particle densimetric Froude number increases monotonically with an increase in transport stage function. However, for a given transport stage function, the variations of mean particle densimetric Froude number with particle parameter do not follow any sequential trend (see the enlarged frame), as was found in the case of relative saltation height (figure 3), relative saltation length (figure 5) and peak particle densimetric Froude number (figure 7). To envision the accurate variation of the mean particle densimetric Froude number F_{dm} with particle parameter $\mathscr{D}$, we consider a random value of transport stage function, say $T = 60$, as shown in the inset of figure 8. It appears that the mean particle densimetric Froude number diminishes with an increase in particle parameter up to $\mathscr{D} = 40$. However, for $\mathscr{D} > 40$, the mean particle densimetric Froude number increases gradually with a further increase in particle parameter.

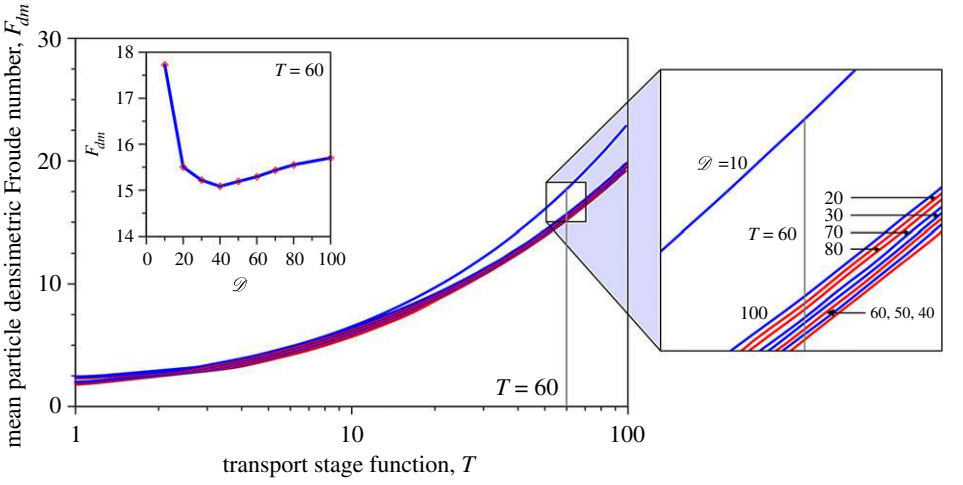

Figure 8. Mean particle densimetric Froude number F_{dm} versus transport stage function T for different values of particle parameter $\mathscr{D}$. In the inset, the variation of mean particle densimetric Froude number F_{dm} with particle parameter $\mathscr{D}$ at a transport stage function T of 60 is shown. (Online version in colour.)

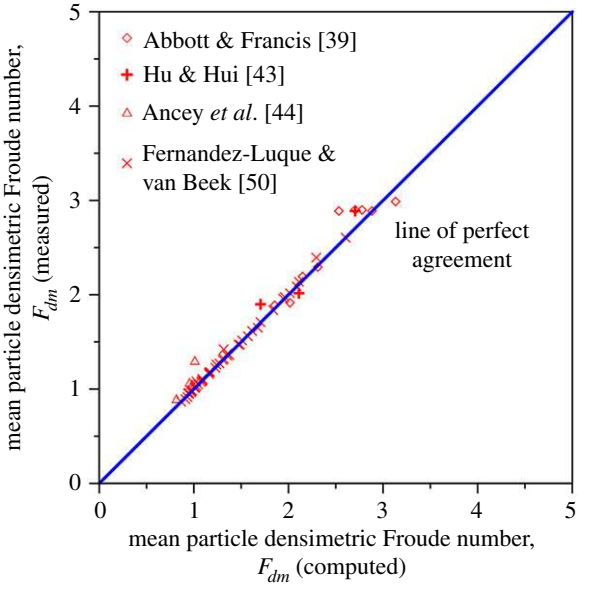

Figure 9. Computed versus measured mean particle densimetric Froude number F_{dm}. (Online version in colour.)

The comparison of the computed mean particle densimetric Froude number F_{dm} with the experimental data of Abbott & Francis [39], Hu & Hui [43], Ancey *et al*. [44] and Fernandez Luque & van Beek [50] is highlighted in figure 9. The computed mean particle densimetric Froude number depicts a satisfactory agreement with the experimental data.

(c) Estimation of bedload flux

The bedload flux Q_b (in volume per unit time and bed width) can be expressed as

$$Q_b = V_p C_v H_s, \tag{3.2}$$

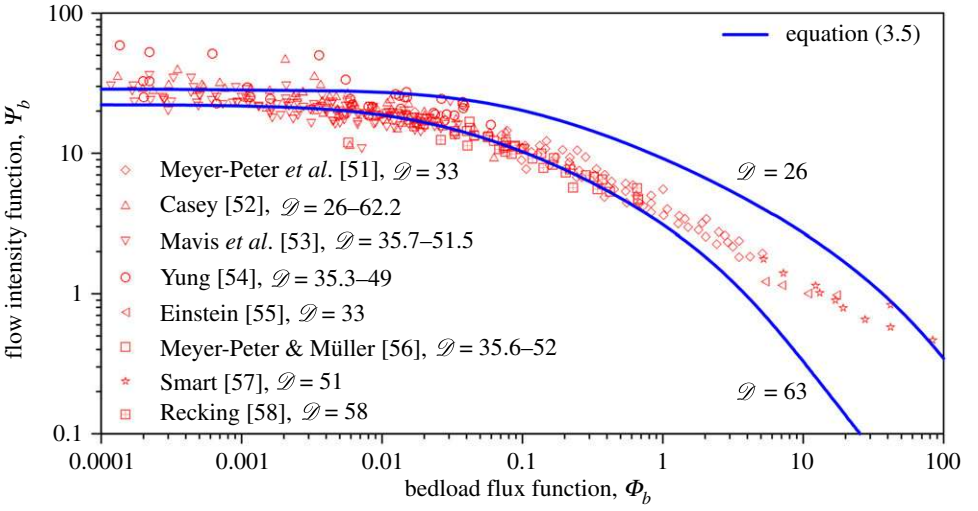

Figure 10. Bedload flux function Φ_b versus flow intensity function Ψ_b. (Online version in colour.)

where V_p is the mean particle velocity during a saltation step and C_v is the volumetric particle concentration within the bedload layer [18]. From the experimental observations, it has been found that the volumetric particle concentration C_v can be expressed as follows [10]:

$$C_v = 0.18 C_0 \frac{T}{\mathscr{D}}, \tag{3.3}$$

where C_0 is the peak bedload concentration (≈ 0.65).

The bedload flux Q_b in dimensionless form, called *bedload flux function*, is expressed as

$$\Phi_b = \frac{Q_b}{\left[\left((\rho_p/\rho_f) - 1\right) g d^3\right]^{1/2}}. \tag{3.4}$$

Substituting equation (3.2) into equation (3.4) and using equation (3.3) yield the bedload flux function Φ_b as

$$\Phi_b = 0.12 \frac{V_p}{\left[\left((\rho_p/\rho_f) - 1\right) g d\right]^{1/2}} \frac{H_s}{d} \frac{T}{\mathscr{D}}. \tag{3.5}$$

In equation (3.5), the mean particle velocity V_p and relative saltation height H_s/d are functions of transport stage function T. For a given particle size, the threshold Shields number Θ_c is a constant. Therefore, from equation (3.5), it appears that for a given particle size, the bedload flux function Φ_b is a function of Shields number Θ or equivalently the *flow intensity function* $\Psi_b (= \Theta^{-1})$. This functional dependency is traditionally expressed as $\Phi_b(\Psi_b)$ [18], where the bedload flux function follows a decreasing trend with an increase in flow intensity function.

Figure 10 illustrates the bedload flux function Φ_b as a function of flow intensity function Ψ_b considering the ample experimental data ranging from particle parameters $\mathscr{D} = 26$ to $\mathscr{D} = 63$ [51–58]. It is worth noting that equation (3.5) allows us to construct the $\Phi_b(\Psi_b)$ curve for any value of particle parameter. However, in order to find the domain of dependency of $\Phi_b(\Psi_b)$ curves on the particle parameter, the computed $\Phi_b(\Psi_b)$ curves for given particle parameters as $\mathscr{D} = 26$ and 63 (that is, $d = 1.03$ and 2.5 mm, respectively) are depicted in figure 10. It is revealed that the experimental data ($26 \leq \mathscr{D} \leq 62.2$) are almost confined to the $\Phi_b(\Psi_b)$ curves corresponding to particle parameters $\mathscr{D} = 26$ and 63, providing the upper and lower bound curves, respectively. It ascertains that equation (3.5) can adequately predict the bedload flux for a wide range of sediment size. Figure 10 reveals that for a given particle parameter, the bedload flux function increases with a decrease in flow intensity function, because of the reduction in applied bed shear stress.

In addition, for a given flow intensity function, the bedload flux function increases as the particle parameter decreases. The underlying reason is due to the fact that for a given applied bed shear stress, the bedload flux function for a finer particle is larger than that for a coarser particle.

4. Conclusion

The mechanics of bed particle saltation in turbulent wall-shear flow is explored by analysing the force system on a saltating particle. The motivating forces, such as the hydrodynamic drag, hydrodynamic lift and the Basset force acting on a saltating particle are analysed from the micro-mechanical perspective. The set of equations controlling the trajectory of particle saltation is solved numerically subject to suitable boundary conditions. The results obtained from mathematical analysis of bed particle saltation are projected to determine the bedload flux. The key conclusions of this study are as follows:

(i) For the particle size range 0.79–3.95 mm (sand to gravel size), the transport stage function equalling unity closely corresponds to the threshold of bed particle saltation. At the threshold of bed particle saltation, the saltation height and saltation length become approximately 1.3 and 9 times the particle size.
(ii) For a given transport stage function, the relative saltation height and relative saltation length reduce with an increase in particle size. In addition, for a given particle size range 0.79–3.95 mm, the relative saltation height and relative saltation length increase as the transport stage function increases, attaining their peaks and then, they decrease with a further increase in transport stage function.
(iii) For a given particle size, the peak and mean particle densimetric Froude numbers depict an increasing trend with the transport stage function. In addition, the curves of peak and mean particle densimetric Froude number as a function of transport stage function for the particle size range 0.79–3.95 mm form a thin band. For the same particle size range with a transport stage function equalling 30, the peak particle densimetric Froude number becomes independent of the particle size. Furthermore, for a transport stage function below 30, the peak particle densimetric Froude number increases with an increase in particle size, while for a transport stage function above 30, it reduces as the particle size increases. On the other hand, for a given transport stage function, the variations of mean particle densimetric Froude number with particle size do not appear to obey any chronological trend.
(iv) The computed bedload flux curves for particle sizes 1.03 and 2.5 mm provide the upper and lower bound curves, respectively, because the experimental data corresponding to this range are nearly limited to the bound curves. For a given particle size, the bedload flux function increases with a decrease in flow intensity function. In addition, for a given flow intensity function, the bedload flux function increases as the particle size decreases.

In essence, this study offers an insightful glance into the mechanics of bed particle saltation in turbulent wall-shear flow by considering an improved version of the force system. The key parameters, evolved from the mathematical analysis, help to obtain an enriched understanding of the mechanics of bed particle saltation. The quintessential element of this study, being largely unexplored in previous analytical studies, opens up a new way of exploring the mechanics of bed particle saltation by expanding the frontier of the present state of the art. The promising synergy between the theoretical results of this study and the experimental observations not only provides an improved design guideline but also makes the mathematical analysis applicable to field situations. It is worth discussing that the present mathematical analysis does not consider explicitly the effects of particle collision, which may become important for high particle transport rate. Therefore, the particle–particle interaction, in addition to the fluid–particle interaction, needs to be addressed in the mathematical formulation as a future scope of research.

Ethics. This study does not include any contents regarding animals or human subjects.

Data accessibility. The source code and the data used in this article can be accessed via this link: https://drive.google.com/file/d/1KyQKTrxy3gZH7FSFARG9RW0TDGfH6ZRn/view?usp=sharing.

Authors' contributions. The conceptualization of the problem including the theoretical foundation was conceived by all the authors. The numerical code, figures and graphics were prepared by E.P. The interpretation of the results and the preparation of the manuscript were done by all three authors. The research was supervised and directed by S.D.

Competing interests. We declare we have no competing interests.

Funding. No funding has been received for this article.

Acknowledgements. S.D. acknowledges the JC Bose Fellowship Award in pursuing this work.

References

1. Ali SZ, Dey S. 2019 Bed particle saltation in turbulent wall-shear flow: a review. *Proc. R. Soc. A* **475**, 20180824. (doi:10.1098/rspa.2018.0824)
2. Shao X, Wu T, Yu Z. 2012 Fully resolved numerical simulation of particle-laden turbulent flow in a horizontal channel at a low Reynolds number. *J. Fluid Mech.* **693**, 319–344. (doi:10.1017/jfm.2011.533)
3. Ji C, Munjiza A, Avital E, Ma J, Williams JJR. 2013 Direct numerical simulation of sediment entrainment in turbulent channel flow. *Phys. Fluids* **25**, 056601. (doi:10.1063/1.4807075)
4. Kidanemariam AG, Uhlmann M. 2014 Direct numerical simulation of pattern formation in subaqueous sediment. *J. Fluid Mech.* **750**, R2. (doi:10.1017/jfm.2014.284)
5. Kidanemariam AG, Uhlmann M. 2017 Formation of sediment patterns in channel flow: minimal unstable systems and their temporal evolution. *J. Fluid Mech.* **818**, 716–743. (doi:10.1017/jfm.2017.147)
6. Chan-Braun C, García-Villalba M, Uhlmann M. 2011 Force and torque acting on particles in a transitionally rough open-channel flow. *J. Fluid Mech.* **684**, 441–474. (doi:10.1017/jfm.2011.311)
7. Ji C, Munjiza A, Avital E, Xu D, Williams J. 2014 Saltation of particles in turbulent channel flow. *Phys. Rev. E* **89**, 052202. (doi:10.1103/PhysRevE.89.052202)
8. Elghannay H, Tafti D. 2018 LES-DEM simulations of sediment transport. *Int. J. Sedim. Res.* **33**, 137–148. (doi:10.1016/j.ijsrc.2017.09.006)
9. Liu D, Liu X, Fu X. In press. LES-DEM simulations of sediment saltation in a rough-wall turbulent boundary layer. *J. Hydraul. Res.* **57**. (doi:10.1080/00221686.2018.1509384)
10. van Rijn LC. 1984 Sediment transport, part I: bed load transport. *J. Hydraul. Eng.* **110**, 1431–1456. (doi:10.1061/(ASCE)0733-9429(1984)110:10(1431))
11. Wiberg PL, Smith JD. 1985 A theoretical model for saltating grains in water. *J. Geophys. Res. Oceans* **90**, 7341–7354. (doi:10.1029/JC090iC04p07341)
12. Wiberg PL, Smith JD. 1989 Model for calculating bed load transport of sediment. *J. Hydraul. Eng.* **115**, 101–123. (doi:10.1061/(ASCE)0733-9429(1989)115:1(101))
13. Niño Y, García M. 1994 Gravel saltation: 2. Modeling. *Water Resour. Res.* **30**, 1915–1924. (doi:10.1029/94WR00534)
14. Lee H-Y, Hsu I-S. 1994 Investigation of saltating particle motions. *J. Hydraul. Eng.* **120**, 831–845. (doi:10.1061/(ASCE)0733-9429(1994)120:7(831))
15. Niño Y, García M. 1998 Using Lagrangian particle saltation observations for bedload sediment transport modelling. *Hydrol. Process.* **12**, 1197–1218. (doi:10.1002/(SICI)1099-1085(19980630)12:8<1197::AID-HYP612>3.0.CO;2-U)
16. Chen Y, Bai Y, Xu D. 2017 On the mechanisms of the saltating motion of bedload. *Int. J. Sedim. Res.* **32**, 53–59. (doi:10.1016/j.ijsrc.2016.07.001)
17. Wang H-W, Lee H-Y, Lee P-N. 2009 Three-dimensional saltating processes of multiple sediment particles. *Int. J. Sedim. Res.* **24**, 16–32. (doi:10.1016/S1001-6279(09)60013-5)
18. Dey S. 2014 *Fluvial hydrodynamics: hydrodynamic and sediment transport phenomena*. Berlin, Germany: Springer.
19. Brush LM, Ho H-W, Yen B-C. 1964 Accelerated motion of a sphere in a viscous fluid. *J. Hydraul. Div.* **90**, 149–160.
20. Owen PR. 1964 Saltation of uniform grains in air. *J. Fluid Mech.* **20**, 225–242. (doi:10.1017/S0022112064001173)
21. White BR, Schultz JC. 1977 Magnus effect in saltation. *J. Fluid Mech.* **81**, 497–512. (doi:10.1017/S0022112077002183)

22. Bialik RJ. 2015 Lagrangian modelling of saltating sediment transport: a review. In *Rivers—physical, fluvial and environmental processes* (eds P Rowiński, A Radecki-Pawlik), pp. 427–441. Berlin, Germany: Springer. (doi:10.1007/978-3-319-17719-9_16)
23. Bagnold RA. 1937 The transport of sand by wind. *Geogr. J.* **89**, 409–438. (doi:10.2307/1786411)
24. Anderson RS, Haff PK. 1988 Simulation of eolian saltation. *Science* **241**, 820–823. (doi:10.1126/science.241.4867.820)
25. Bagnold RA. 1973 The nature of saltation and of 'bedload' transport in water. *Proc. R. Soc. Lond. A* **332**, 473–504. (doi:10.1098/rspa.1973.0038)
26. Francis JRD. 1973 Experiments on the motion of solitary grains along the bed of a water-stream. *Proc. R. Soc. Lond. A* **332**, 443–471. (doi:10.1098/rspa.1973.0037)
27. Dey S, Ali SZ. 2019 Bed sediment entrainment by streamflow: state of the science. *Sedimentology* **66**, 1449–1485. (doi:10.1111/sed.12566)
28. Dey S, Ali SZ. 2018 Review article: advances in modeling of bed particle entrainment sheared by turbulent flow. *Phys. Fluids* **30**, 061301. (doi:10.1063/1.5030458)
29. Cao Z, Pender G, Meng J. 2006 Explicit formulation of the Shields diagram for incipient motion of sediment. *J. Hydraul. Eng.* **132**, 1097–1099. (doi:10.1061/(ASCE)0733-9429(2006)132:10(1097))
30. Ali SZ, Dey S. 2016 Hydrodynamics of sediment threshold. *Phys. Fluids* **28**, 075103. (doi:10.1063/1.4955103)
31. Yen BC. 1992 Sediment fall velocity in oscillating flow. Water Resources and Environmental Engineering Research Report, issue 11. Department of Civil Engineering, University of Virginia, Charlottesville, VA, USA.
32. Taylor GI. 1935 Statistical theory of turbulence. *Proc. R. Soc. Lond. A* **151**, 421–444. (doi:10.1098/rspa.1935.0158)
33. Nezu I, Nakagawa H. 1993 *Turbulence in open-channel flows*. Rotterdam, The Netherlands: Balkema.
34. Saffman PG. 1965 The lift on a small sphere in a slow shear flow. *J. Fluid Mech.* **22**, 385–400. (doi:10.1017/S0022112065000824)
35. Saffman PG. 1968 Corrigendum, the lift on a small sphere in a slow shear flow. *J. Fluid Mech.* **31**, 624. (doi:10.1017/S0022112068999990)
36. Rubinow SI, Keller JB. 1961 The transverse force on a spinning sphere moving in a viscous fluid. *J. Fluid Mech.* **11**, 447–459. (doi:10.1017/S0022112061000640)
37. Nezu I. 1977 Turbulent structure in open channel flow. PhD thesis, Kyoto University, Kyoto, Japan.
38. Grass AJ. 1971 Structural features of turbulent flow over smooth and rough boundaries. *J. Fluid Mech.* **50**, 233–255. (doi:10.1017/S0022112071002556)
39. Abbott JE, Francis JRD. 1977 Saltation and suspension trajectories of solid grains in a water stream. *Phil. Trans. R. Soc. Lond. A* **284**, 225–254. (doi:10.1098/rsta.1977.0009)
40. Niño Y, García M. 1998 Experiments on saltation of sand in water. *J. Hydraul. Eng.* **124**, 1014–1025. (doi:10.1061/(ASCE)0733-9429(1998)124:10(1014))
41. Auel C, Albayrak I, Sumi T, Boes RM. 2017 Sediment transport in high-speed flows over a fixed bed: 1. Particle dynamics. *Earth Surf. Proc. Landf.* **42**, 1365–1383. (doi:10.1002/esp.4128)
42. Auel C, Albayrak I, Sumi T, Boes RM. 2017 Sediment transport in high-speed flows over a fixed bed: 2. Particle impacts and abrasion prediction. *Earth Surf. Proc. Landf.* **42**, 1384–1396. (doi:10.1002/esp.4132)
43. Hu C, Hui Y. 1996 Bed-load transport. I: mechanical characteristics. *J. Hydraul. Eng.* **122**, 245–254. (doi:10.1061/(ASCE)0733-9429(1996)122:5(245))
44. Ancey C, Bigillon F, Frey P, Lanier J, Ducret R. 2002 Saltating motion of a bead in a rapid water stream. *Phys. Rev. E* **66**, 036306. (doi:10.1103/PhysRevE.66.036306)
45. Ramesh B, Kothyari UC, Murugesan K. 2011 Near-bed particle motion over transitionally-rough bed. *J. Hydraul. Res.* **49**, 757–765. (doi:10.1080/00221686.2011.620369)
46. Niño Y, García M, Ayala L. 1994 Gravel saltation: 1. Experiments. *Water Resour. Res.* **30**, 1907–1914. (doi:10.1029/94WR00533)
47. Lee H-Y, Chen Y-H, You J-Y, Lin Y-T. 2000 Investigations of continuous bed load saltating process. *J. Hydraul. Eng.* **126**, 691–700. (doi:10.1061/(ASCE)0733-9429(2000)126:9(691))
48. Chatanantavet P, Whipple KX, Adams MA, Lamb MP. 2013 Experimental study on coarse grain saltation dynamics in bedrock channels. *J. Geophys. Res. Earth Surf.* **118**, 1161–1176. (doi:10.1002/jgrf.20053)

49. Bhattacharyya A, Ojha SP, Mazumder BS. 2013 Evaluation of the saltation process of bed materials by video imaging under altered bed roughness. *Earth Surf. Proc. Landf.* **38**, 1339–1353. (doi:10.1002/esp.3370)
50. Fernandez Luque R, van Beek R. 1976 Erosion and transport of bed-load sediment. *J. Hydraul. Res.* **14**, 127–144. (doi:10.1080/00221687609499677)
51. Meyer-Peter E, Favre H, Einstein HA. 1934 Neuere versuchsresultate über den geschiebetrieb. *Schweiz. Bauztg.* **103**, 147–150.
52. Casey HJ. 1935 Über geschiebebewegung. In *Mitteilungen der Preussischen Versuchsanstalt für Wasserbau und Schiffbau*, Berlin, Germany.
53. Mavis FT, Liu T, Soucek E. 1937 *The transportation of detritus by flowing water-II*. University of Iowa: Iowa, USA.
54. Yung HP. 1939 Abhangigkeit der geschiebebewegung von der kornform und der temperature. In *Mitteilungen der Preussischen Versuchsanstaltt für Wasserbau und Schiffbau*, Berlin, Germany.
55. Einstein HA. 1942 Formulas for the transportation of bed load. *Trans. Am. Soc. Civ. Eng.* **107**, 561–577.
56. Meyer-Peter E, Müller R. 1948 Formulas for bed-load transport. In *Proc. of the 2nd Meeting of Int. Association for Hydraulic Research, Stockholm, Sweden, 7–9 June*, vol. 3, pp. 39–64. Madrid, Spain: IAHR.
57. Smart GM. 1984 Sediment transport formula for steep channels. *J. Hydraul. Eng.* **110**, 267–276. (doi:10.1061/(ASCE)0733-9429(1984)110:3(267))
58. Recking A. 2006 An experimental study of grain sorting effects on bedload. PhD thesis, University of Lyon, Lyon, France.